Geosciences Journal
Vol. 20, No. 5, p. 705 − 718, October 2016
DOI 10.1007/s12303-016-0003-3

Landslide susceptibility mapping at Gongliu county, China using artificial neural network and weight of evidence models

Qiqing Wang
Wenping Li*
Maolin Xing
Yanli Wu
Yabing Pei
Dongdong Yang
Hanying Bai

School of Resources and Earth Science, China University of Mining and Technology, Xuzhou 221116, China

College of Earth Sciences, Guilin University of Technology, Guilin 541004, China

ABSTRACT: The aim of this study was to apply and to verify the use of artificial neural network (ANN) and weight of evidence (WoE) models to landslide susceptibility mapping in the Gongliu county, China, using a geographic information system (GIS). For this aim, in this study, a landslide inventory map was prepared using earlier reports and aerial photographs as well as by carrying out field surveys. A total of 163 landslides (70% out of 233 detected landslides) were randomly selected for model training, and the remaining 70 landslides (30%) were used for the model validation. Then, a total number of twelve landslide conditioning factors, such as slope angle, slope aspect, general curvature, plan curvature, profile curvature, altitude, distance to rivers, distance to roads, lithology, rainfall, normalized difference vegetation index (NDVI), and sediment transport index (STI), were used in the analysis. Landslide hazardous areas were analyzed and mapped using the landslide-occurrence factors by ANN and WoE models. Finally the output maps were validated using the area under the curve (AUC) method. The validation results showed that the ANN model with a success rate of 82.51% and predictive accuracy of 77.31% performs better than WoE (success rate, 79.82%; predictive accuracy, 74.59%) model. Overall, both models showed almost similar results. Therefore, the two landslide susceptibility maps obtained were successful and can be useful for preliminary general land use planning and hazard mitigation purpose.

Key words: landslide, susceptibility mapping, artificial neural network (ANN), weight of evidence (WoE), China

1. INTRODUCTION

Landslides, causing extensive damages to residential regions, economic losses, and human casualties all over the world, are one of the most significant natural damaging disasters in hilly environments due to the steep topography, improper use of land cover and adverse climatic conditions for landslides (Akgun et al., 2008; Sujatha et al., 2012; Solaimani et al., 2013; Ahmed, 2014). Globally, landslides cause approximately 1,000 deaths per year and property damage of about 4 billion dollars (Lee and Pradhan, 2007). China is one of the countries in the world mostly affected by landslides, which often result in large numbers of casualties and huge economic losses. It is reported that more than 30,737 hazards associated with landslides occurred in 2012, 2013 and 2014, which caused a total of 1,256 people dead or missing, and a direct economic loss of 15.41 billion CNY (http://www.cigem.gov.cn). To minimize the losses of human life and economic value, potential landslide-prone areas should be identified (Devkota et al., 2013; Pourghasemi et al., 2013a).

The landslide susceptibility means the likelihood (probability) of damaging landslide occurrence with statistical sense (Yang et al., 2015). So far, numerous methodologies have been developed to assess and map landslide susceptibility (Akgun et al., 2008; Wu and Chen, 2009; Solaimani et al., 2013; Wang et al., 2015). Probabilistic models, such as the frequency ratio, weight of evidence models etc. have been proposed (Lee and Choi, 2004; Lee and Sambath, 2006; Lee and Pradhan, 2007; Akgun et al., 2008; Yilmaz, 2009; Regmi et al., 2010; Pradhan and Lee, 2010c; Xu et al., 2012). The logistic regression model has also been applied to landslide susceptibility mapping (Ohlmacher and Davis, 2003; Ayalew and Yamagishi, 2005; Lee, 2005a; Lee and Pradhan, 2007; Yilmaz, 2009). Data mining using fuzzy logic, artificial neural network and decision tree models have also been applied in geographical information systems (GIS) as a new landslide susceptibility assessment method (Lee et al., 2003, 2004; Ermini et al., 2005; Gorsevski et al., 2006; Biswajeet and Saro, 2007; Yilmaz, 2009; Saito et al., 2009; Yeon et al., 2010; Nefeslioglu et al., 2010; Pradhan, 2011a, b; Pourghasemi et al., 2012; Tien Bui et al., 2012; Bui et al., 2012a; Pradhan, 2013). Additionally, In order to find the better model that is more accurate in landslide susceptibility mapping in a study area, some studies have used two or three models and compare their accuracy such as probability and statistical analyses, probability and fuzzy-logic analyses, statistical and ANN analyses, analytic hierarchy process, probability and statistical analyses, and probability, statistical, and ANN analyses etc. (Lee and Pradhan, 2007; Pouydal et al., 2010; Constantin et al., 2011; Kanungo et

*Corresponding author: wpligroup@126.com

al., 2011; Yalcin et al., 2011; Akgun, 2012; Demir et al., 2013; Devkota et al., 2013; Ozdemir and Altural, 2013; Park et al., 2013; Pourghasemi et al., 2013b; Solaimani et al., 2013; Youssef et al., 2014a; Jaafari et al., 2014). The main difference between this study and the references is that artificial neural network and weight of evidence models were applied and compared for the landslide susceptibility mapping on the Gongliu county of China.

This paper attempts to produce landslide susceptibility maps of Gongliu county in Xinjiang Uygur Autonomous Region, China, using a geographical information system (GIS). To achieve this aim, the artificial neural network (ANN) and weight of evidence (WoE) models to obtain the landslide susceptibility maps using the ArcGIS 10.0 software (ESRI Inc., Redlands, CA, USA) were developed, applied, and verified in the study area.

2. STUDY AREA

The study area, in Xinjiang Uygur Autonomous Region, consisted of approximately 4,124 km^2 located between 81°34′ and 83°35′ west-east longitudes and 42°54′ and 43°38′ north-south latitudes in the northwestern part of China (Fig. 1). The climate of this region is characterized by the typical continental semi-arid climate, the winter is dry and cold, but the summer is hot and rainy. The temperature of the area varies between –37 °C in winter and 39 °C in summer with a yearly average of 7.4 °C. The mean annual rainfall according to local weather station in a period of 40 years is around 200–700 mm, and the most rainfall appears in April to July (C.H. of China Meteorological Administration (CMA) 2014). The altitude of the area ranges from 767 to 4,217 m asl and the major terrain can be classified into three regions: the plain region,

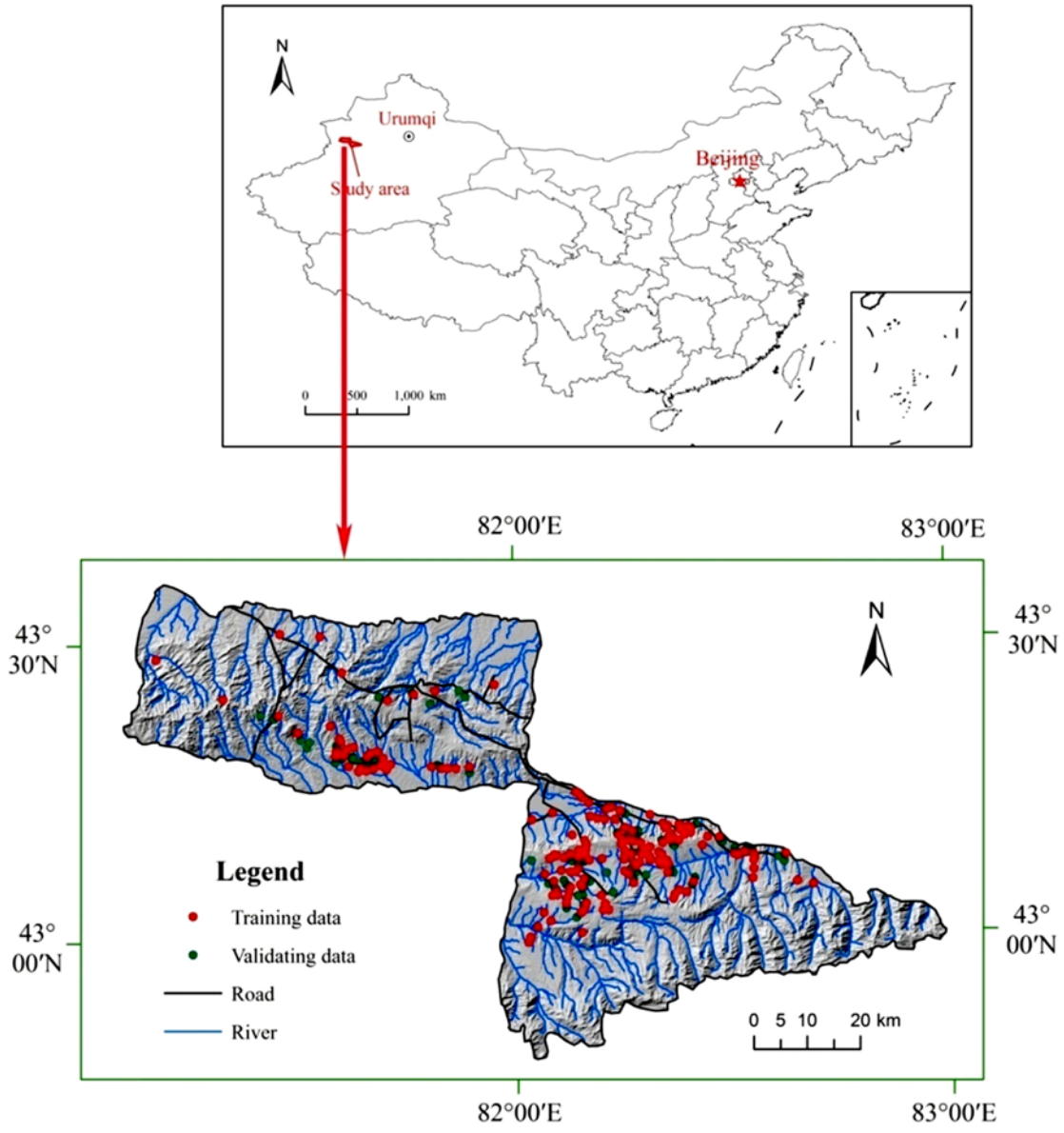

Fig. 1. The study area with landslide locations.

the mountain region, and the hill region. Mountainous and hilly region accounted for about 72.6% of the total area. The main streams in the region are Langhe and Nanshan Rivers, and these rivers and their tributaries form dentritic drainage system due to topographical and geological features of the area. The traffic of this area mainly is high way. The population of the county was about 196,400 in 2011 year. Major settlements are mainly distributed in the middle of area. This site is one of the frequent landslide occurrence areas in China due to the coupling effects of special geological and climatic conditions and the influences of human engineering activities. In total, 233 landslides were identified and mapped in the study area.

3. DATA PREPARATION

3.1. Landslide Inventory Map

The landslide inventory map is essential for the landslide susceptibility analysis, which can provide information for the assessment of the influence of different conditioning factors on landslide occurrence (van Westen et al., 2006; Solaimani et al., 2013; Pradhan and Kim, 2014; Youssef et al., 2014b). The reliability and accuracy of the collected data related to landslides affect the success of landslide susceptibility analysis. In this study, the landslide inventory map of the region was prepared by using 1:50,000 scale aerial-photo interpretation and extensive field surveys. In addition, the historical landslides records obtained from the internet and published literature were also used (Qin, 2007). A total of 233 landslides were identified, as shown in Figure 1, 163 (70%) of which were randomly selected as training data and the remaining 70 (30%) were kept for validation purposes. All data layers were transformed in raster format with pixel size of 30 × 30 meters, hence the area grid was 3,356 rows by 5,830 columns with a total of 6,430,157 pixels.

3.2. Thematic Layers

There were twelve landslide conditioning factors (slope angle, slope aspect, general curvature, plan curvature, profile curvature, altitude, distance to rivers, distance to roads, lithology, rainfall, NDVI, STI) considered in the analyses performed in the present study. In this study, a 30 m × 30 m digital elevation model (DEM) was collected from the Advanced Spaceborne Thermal Emission and reflection radiometer (ASTER). From this DEM, geomorphological thematic data layers, such as slope angle, slope aspect, general curvature, plan curvature, profile curvature, and altitude maps, were prepared. Other parameters were mainly collected from available resources (geological map, environment geology map, road map and drainage map etc.). All of these data were produced in raster format with a pixel size of 30 × 30 m^2 to be compatible with the spatial resolution.

Slope angle, with direct effect on landslide formation, is frequently used in landslide susceptibility studies (Dai et al., 2001; Dragićević et al., 2015). Slope aspect is the direction of maximum slope of the terrain surface (Kayastha et al., 2013a). The aspect is also an important factor in landslide susceptibility studies since aspect affects parameters such as rainfall, discontinuities and exposure to sunlight (Süzen and Doyuran, 2004; He et al., 2012). Commonly, general curvature, defined as the rate of change of slope degree or aspect, has been argued to affect slope stability. The characterization of slope morphology and flow can be analyzed with the help of the general curvature map (Nefeslioglu et al., 2008). The plan curvature is described as the curvature of a contour line formed by intersection of a horizontal plane with the surface. The profile curvature is the vertical plane parallel to the slope direction (Kannan et al., 2013). Plan curvature influences the convergence and divergence of flow across a surface. Profile curvature affects the acceleration and deceleration of downslope flows and, as a result, influences erosion and deposition (Pourghasemi et al., 2013a; Kritikos and Davies, 2015). In the present study, the slope angle, slope aspect, general curvature, plan curvature, and profile curvature were calculated in ArcGIS 10.0 based on DEM data. The slope angle was divided into seven categories (Fig. 2a) considering the steepness of the terrain (Kayastha et al., 2013b; Liu et al., 2014). The aspect was classified into nine directional classes as flat (–1), north (337.5–360, 0–22.5), northeast (22.5–67.5), east (67.5–112.5), southeast (112.5–157.5), south (157.5–202.5), southwest (202.5–247.5), west (247.5–292.5), and northwest (292.5–337.5) (Fig. 2b). The general curvature, plan curvature and profile curvature were divided into three classes, respectively (Figs. 2c–e).

The altitude or elevation does not contribute directly to landslide manifestation, but in relation to the other parameters, like tectonics, erosion-weathering processes, and precipitation, the altitude contributes to landslide manifestation and influences the whole system (Ercanoglu et al., 2004; Rozos et al., 2011). In this study, the elevation ranges from 767 to 4,217 m and was divided into five classes using an interval of 600 m (Fig. 2f).

Two proximity parameters including distance to rivers and distance to roads were taken into account in the study. Rivers/streams may adversely affect stability of the materials by eroding the toe of the slopes or by saturating the lower part of material unit resulting in water level increases. Generally speaking, landslide frequency decreases as distance to rivers increases (Dai and Lee, 2002; Youssef, 2015; Dragićević et al., 2015). The distance to rivers was calculated by Euclidean distance tool of ArcGIS 10.0 and reclassified the resultant map into five classes (Fig. 2g): 0–200, 200–400, 400–600, 600–800, and >800 m. The distance to roads is one of the causal factors for landslides and is parallel to the effect of the distance to rivers. The load in the toe of slope can be reduced by road-cuts (Yalcin et al., 2011). In the present study, five

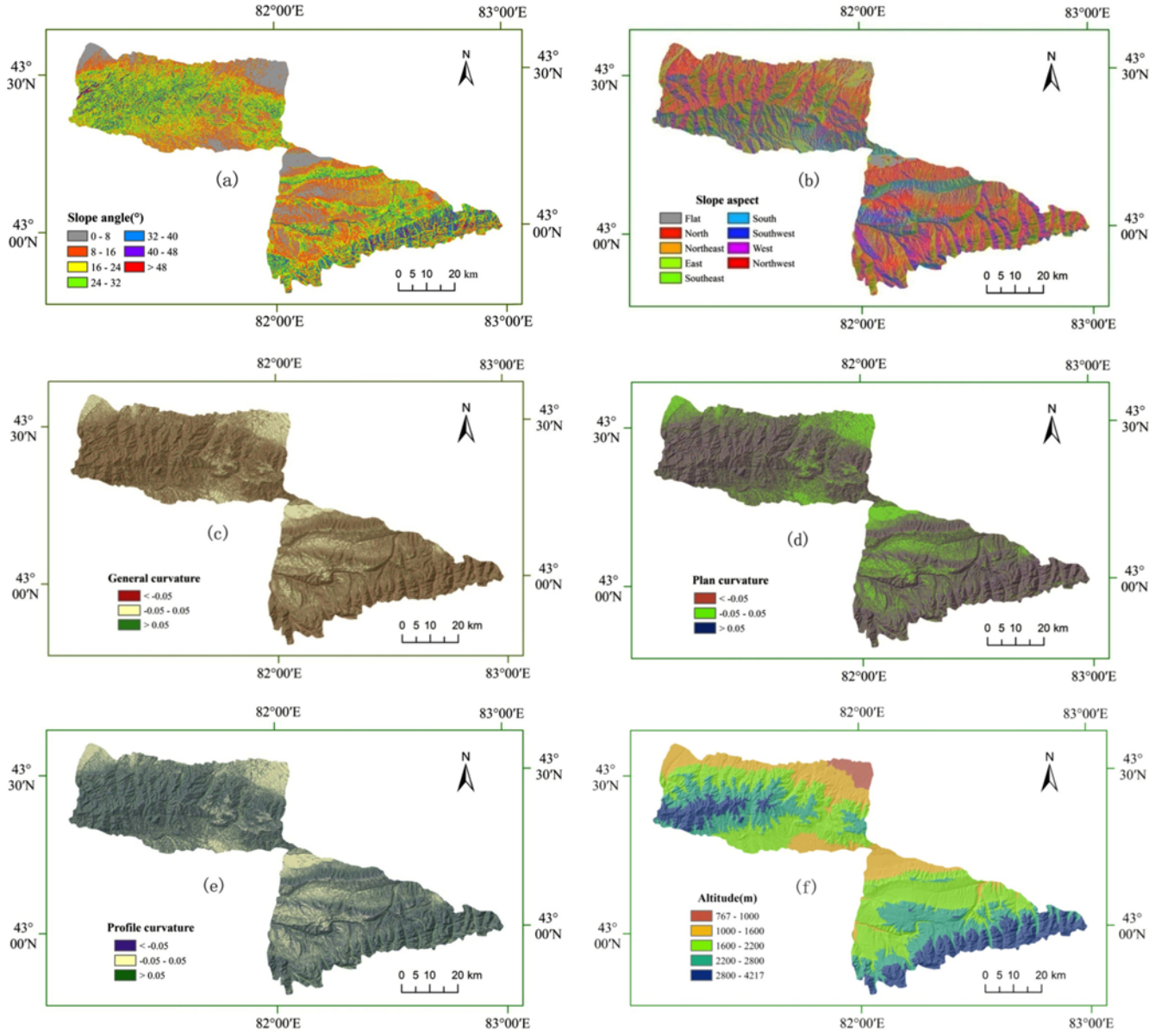

Fig. 2. Landslide conditioning factors of the study area: (a) slope angle, (b) slope aspect, (c) general curvature, (d) plan curvature, (e) profile curvature, (f) altitude.

different buffer zones were created within the study area to determine the degree to which the roads affected the slopes (Fig. 2h).

Lithology is one of the most important parameters for landslide susceptibility analysis since landslides are controlled by the rock properties of the land surface and different lithological units have different susceptibility values (Yesilnacar and Topal, 2005; Yalcin et al., 2011). For the current study, a lithological map was extracted from the geology database of the area. The study area is covered with various types of lithological units. Their names, lithologic characteristics, and ages of the geological units are provided in Table 1, and the general geological setting of the area is shown on the source map (Fig. 2i).

Precipitation, in particular sudden, intense rain and snow melt, is a very important controlling factor which triggers mass movements, increasing the underground hydrostatic level and water pressure (Van Westen et al., 2006; Shahabi et al., 2014; Yang et al., 2015). In the present study, the average annual rainfall was used to characterize the precipitation factor. The annual rainfall of the study area is shown as Figure 2j, and reclassified into five classes: <300, 300–400, 400–500, 500–600, >600 mm/year.

The NDVI is often considered as a controlling factor in landslide susceptibility mapping. In general, the higher the value of NDVI is, the larger the area that is covered by vegetation. Also, the relatively low vegetation coverage can easier lead to landslide incidence (He et al., 2012; Youssef, 2015).

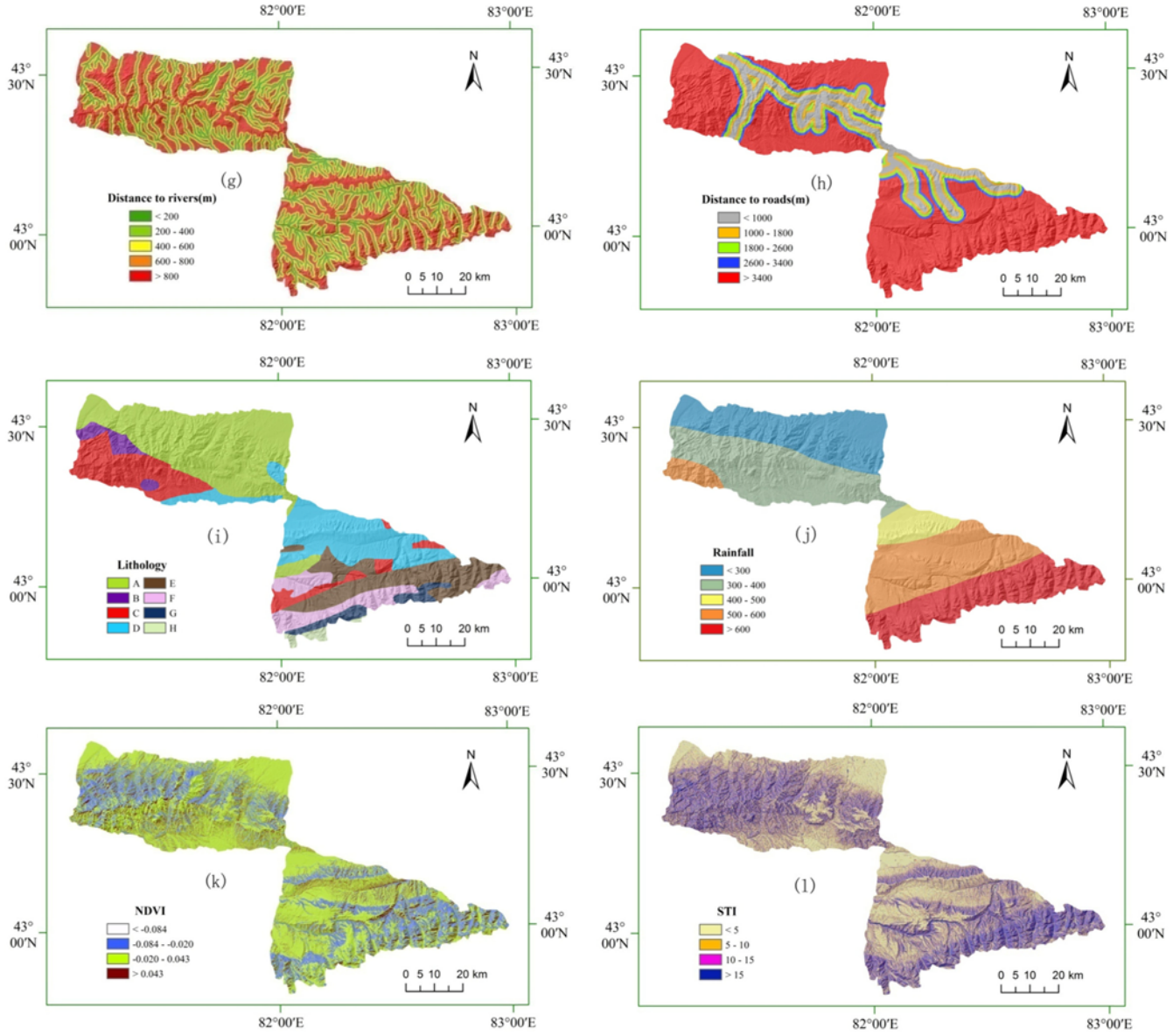

Fig. 2. (continued). (g) distance to rivers, (h) distance to roads, (i) lithology, (j) rainfall, (k) NDVI, and (l) STI.

Table 1. Description of geological units of the study area (Qin, 2007)

No.	Formation	Code	Lithology
A	–	Q_h, Q_p	Cohesive soil, sand gravel, pebbles, loess and gravel
B	Wulang, Shuixi Xiaoquangou	P_1, $J_{1–2}$, $T_{2–3}$	Argillaceous siltstone, sandstone, quartz sandstone, quartzite, mudstone, carbonaceous mudstone
C	Tuokuzidaban, Ishrick	C_1, T C_2	Conglomerate, limestone, siltstone, volcanic clastic limestone, sandy shale, clay shale
D	Akshak, Dahalajunshan	C_1, Q_p	Carbonate, clastic rocks, glutenite, limestone, rhyolitic porphyry, basaltic porphyrite
E	Shawan	D	Granite, granodiorite, plagioclase granite, granite porphyry, diorite
F	The Permian granite, Tekes	P	Monzonitic granite, intermediate-acid igneous rocks, neutral volcanic clastic rock
G	Xingditag, Tekes	C_h, P_t	Quartzite, quartz-schist, siltstone, phyllite, limestone and marble rock
H	Keketiekedaban	S	Limestone, pyroclastic rocks, monzonitic granite

In this study, the NDVI map was obtained from Landsat7 ETM$^+$ satellite image acquired on 12 November 2010. The NDVI value was calculated using the formula:

$$NDVI = (IR - R)/(IR + R), \quad (1)$$

where IR is the infrared portion of the electromagnetic spec-

trum, and *R* is the red portion of the electromagnetic spectrum (Youssef et al., 2014a). Finally, the four classes of the NDVI were extracted as Figure 2k.

The sediment transport index (STI) characterizes the process of erosion and deposition (Devkota et al., 2013). The STI is calculated from the following formula:

$$STI = \left(\frac{As}{22.13}\right)^{0.6}\left(\frac{\sin\beta}{0.0896}\right)^{1.3}, \quad (2)$$

where A_S is the specific catchment's area (m^2/m), and β the slope gradient. In this study, STI was considered as another conditioning factor and divided into four classes <5, 5–10, 10–15, >15 (Fig. 2l).

4. MODELING APPROACH

4.1. Artificial Neural Network (ANN) Model

An artificial neural network (ANN) is a "computational mechanism able to acquire, represent, and compute a mapping from one multivariate space of information to another, given a set of data representing that mapping" (Garrett, 1994; Pradhan and Lee, 2010a). There are many kinds of ANN models, among which multi-layer perceptron (MLP) is perhaps the most popular and most widely used ANN architecture (Bui et al., 2012b; Polykretis et al., 2015). In this study, the MLP Neural Nets is a feed-forward neural network trained by the backwards propagation (BP) algorithm, consisting of an input layer, hidden layers, and an output layer (Fig. 3). The basic mathematical concepts of the back-propagation algorithm are found in Hush and Horne (1993). In this specific case, there are 12 input neurons (one each for slope angle, slope aspect, general curvature, plan curvature, profile curvature, altitude, distance to rivers, distance to roads, lithology, rainfall, NDVI, STI) and the output layer will have two neurons. Sandwiched between the input and output layers is the hidden layer consist of one or more neurons that are determined based on the training data. Each neuron in the hidden layer was interconnected to neurons in both the preceding and following layers by weighted connections and non-linear activation functions are used to propagate information between these layers (Pradhan and Lee, 2010b; Choi et al., 2012). The weight adjustment is controlled by the momentum and learning rate factors during the training phase (Bagher-Ebadian et al., 2009).

There are two stages involved in using neural networks for multi-source classification: the training stage, in which the internal weights are adjusted, and the classifying stage. Typically, the back-propagation algorithm trains the network until some targeted minimal error is achieved between the desired and actual output values of the network. When the training is complete, the network is used as a feed-forward structure to produce a classification for the entire dataset (Paola and Schowengerdt, 1995; Pradhan and Lee, 2010b). In this process, each hidden and output layer neuron processes its inputs by multiplying each input (x_i) by a corresponding weight (w_i), summing the product Equation (3), and then processing the sum (if that exceeds the neuron threshold, then the neuron is activated) using a non-linear activation function, Equation (4), to produce a result (y_i) (Polykretis et al., 2015).

$$net = \sum_{i=0}^{n} w_i x_i, \quad (3)$$

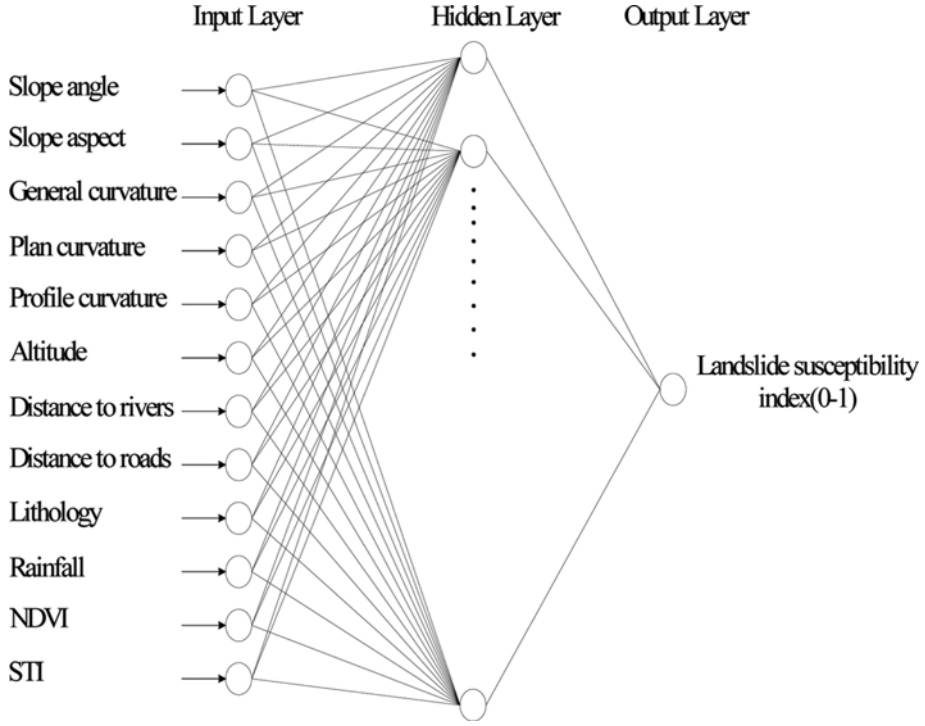

Fig. 3. Architecture of neural network model used in the study.

$$y_i = f(net)\,. \quad (4)$$

Generally, the number of hidden layers and the number of nodes in a hidden layer required for a particular classification problem are not easy to deduce. In this study, the neuron number of the hidden layer was 25 when calculated by the equation suggested by Hecht-Nielsen (1987). Therefore, a 12 (input layers) × 25 (hidden layers) × 2 (output layers) structure was selected for the network, with input data normalized in the range of 0.1–0.9 (Pradhan and Lee, 2010c). The nominal and interval class group data were converted to continuous values ranging between 0.1 and 0.9. The learning rate was set at 0.01, and the initial weights were randomly selected. The root mean-square error (RMSE) goal for the stopping criterion was set to 0.01. The final weights between layers acquired during training of the neural network and the contribution or importance of each of the twelve factors were used to predict landslide susceptibility.

4.2. Weights of Evidence (WoE) Model

The weight of evidence (WoE) model is based on Bayesian probability framework, which was originally developed for mineral potential assessment (Agterberg et al., 1993; Bonham-Carter et al., 1988; Dahal et al., 2008). The method has later been adapted by several workers in landslide susceptibility mapping (van Westen, 2000; Lee et al., 2002; Dahal et al., 2008; Regmi et al., 2010). A detailed description of the mathematical formulation of the model is available in several research papers (Bonham-Carter et al., 1988; van Westen, 2000; Lee et al., 2002; Dahal et al., 2008; Regmi et al., 2010). The WoE model is fundamentally based on the calculation of positive and negative weights W^+ and W^-. The model calculates the weight for each landslide predictive factor (B) based on the presence or absence of the landslides (D) within the area as follows (Dahal et al., 2008):

$$W_i^+ = \ln\frac{P\{B|D\}}{P\{B|\overline{D}\}}, \quad (5)$$

$$W_i^- = \ln\frac{P\{\overline{B}|D\}}{P\{\overline{B}|\overline{D}\}}, \quad (6)$$

where P is the probability and ln is the natural log. Similarly, B is a class of the particular predictive variable and the $\overline{B}$ represents the absence of the class and/or of the event (landslide). D is the presence of landslide, and $\overline{D}$ is the absence of a landslide. A positive weight (W_i^+) indicates that the predictable variable is present at the landslide locations. and the magnitude of this weight is an indication of the positive correlation between presence of the predictable variable and landslides. A negative weight (W_i^-) indicates the absence of the predictable variable and shows the level of negative correlation (Dahal et al., 2008). The difference between the two weights is known as the weight contrast,

$$C = W_i^+ - W_i^-, \quad (7)$$

which provides a measure of the strength of the correlation between the predictable variable and landslides (Armaş, 2012). The variance of the contrast, $S^2(C)$, is given by the sum of $S^2(W^+)$, and $S^2(W^-)$, and the studentised contrast, $C/S(C)$, gives a measure of confidence (Kayastha et al., 2012).

5. RESULTS AND DISCUSSION

5.1. Artificial Neural Network (ANN) Model

In this study, the results of frequency ratio for different classes of the conditioning factors were shown in Table 2, which show the importance of the respective classes in the slope instability. It can be observed from Table 2 that the slope angle class 0–16 has the higher frequency ratio value (>1), which indicates a high probability of landslide occurrence. From this, the landslide occurrence decreases by the increase in slope gradient. The reason for this circumstance may be that the resistant lithologic units exist in the gentle slopes and they are not covered by highly and completely weathered lithologic units, which are susceptible to landsliding (Akgun et al., 2008; Yalcin et al., 2011). In the case of slope aspect, most of the landslides occurred in south facing. The frequency ratio values of general curvature, plan curvature, and profile curvature show that the frequency ratio values for each class were similar, which indicates that these classes have no obvious effect on the occurrence of landslides. In the case of altitude, both 1,600–2,200 m classes have 66.87% of landslide probability and frequency ratio value of 1.77. Assessment of distance from rivers and roads showed that distance of 200–400 m of rivers and 0–1,000 m of roads have high correlation with landslide occurrence. In the case of the lithology, it can be seen that the lithology class D has highest frequency ratio value (3.28). This indicates that lithological unit of the carbonate, clastic rocks, glutenite, limestone, rhyolitic porphyry, and basaltic porphyrite has the highest influence in triggering landslides. For the rainfall, the results show that the frequency ratio values in classes of 400–500, 500–600 mm/year are very high than that of the other three classes. In addition, the NDVI factor shows that the range <–0.084 and >0.043 is relatively unfavorable (non-susceptible) and favorable (high susceptible) for landslide occurrence. The main reason for this is that other conditioning factors, such as altitude, distance to roads, lithology, and rainfall, play a more important role in landslide occurrence comparing to the NDVI factor in this study area. The relation between STI and landslide probabilities showed that <5 class has the highest frequency ratio value (1.34).

For visual interpretation of landslide susceptibility index map, the data need to be classified into categorical susceptibility classes (Jaafari et al., 2014). Various classifier systems exist such as natural breaks, quantiles, equal intervals, and standard

deviation (Ayalew and Yamagishi, 2005). The natural break method has been widely used in the various literatures (Akgun et al., 2012; Pourghasemi et al., 2012, 2013c; Jaafari et al., 2014; Shahabi et al., 2014). Generally, this method could be chosen if the data distribution has a positive or negative skewness (Jaafari et al., 2014). In this study, considering data distribution histogram, landslide susceptibility map was classified into five categories by using the natural break method of ArcGIS 10.0. These categories include five classes of very low, low, moderate, high, and very high (Fig. 4). 16.58 and 24.37% of the total area are found under very low and low landslide susceptibility classes. Areas covering moderate, high

Table 2. Spatial relationship between each landslide conditioning factor and landslide for each model

Factors	Classes	Percentage of landslide (%)	Percentage of domain (%)	Frequency ratio	W^+	W^-	C	$S(C)$	$C/S(C)$
Slope angle (°)	0–8	36.81	24.90	1.48	0.39	–0.17	0.56	0.16	3.47
	8–16	26.99	21.93	1.23	0.21	–0.07	0.28	0.18	1.56
	16–24	20.25	21.34	0.95	–0.05	0.01	–0.07	0.20	–0.34
	24–32	10.43	16.82	0.62	–0.48	0.07	–0.55	0.26	–2.15
	32–40	4.29	10.23	0.42	–0.87	0.06	–0.93	0.39	–2.41
	40–48	1.23	3.85	0.32	–1.14	0.03	–1.17	0.71	–1.64
	>48	0.00	0.94	0.00	0.00	0.01	0.00	0.00	0.00
Slope aspect	Flat	10.43	9.18	1.14	0.13	–0.01	0.14	0.26	0.55
	North	9.20	12.86	0.72	–0.34	0.04	–0.38	0.27	–1.39
	Northeast	13.50	14.16	0.95	–0.05	0.01	–0.06	0.23	–0.24
	East	11.66	12.25	0.95	–0.05	0.01	–0.06	0.24	–0.23
	Southeast	9.20	9.21	1.00	0.00	0.00	0.00	0.27	0.00
	South	11.04	7.49	1.47	0.39	–0.04	0.43	0.25	1.71
	Southwest	11.66	9.91	1.18	0.16	–0.02	0.18	0.24	0.75
	West	12.88	11.96	1.08	0.07	–0.01	0.09	0.23	0.36
	Northwest	10.43	12.98	0.80	–0.22	0.03	–0.25	0.26	–0.97
General curvature	<–0.05	40.49	40.16	1.01	0.01	–0.01	0.01	0.16	0.09
	–0.05–0.05	19.63	20.25	0.97	–0.03	0.01	–0.04	0.20	–0.20
	>0.05	39.88	39.59	1.01	0.01	–0.01	0.01	0.16	0.07
Plan curvature	<–0.05	32.52	35.30	0.92	–0.05	0.03	–0.08	0.16	–0.51
	–0.05–0.05	37.42	28.89	1.30	–0.14	0.07	–0.20	0.16	–1.24
	>0.05	30.06	35.82	0.84	0.20	–0.09	0.29	0.16	1.86
Profile curvature	<–0.05	39.26	35.20	1.12	0.11	–0.07	0.17	0.16	1.08
	–0.05–0.05	30.06	28.32	1.06	0.06	–0.03	0.08	0.17	0.49
	>0.05	30.68	36.48	0.84	–0.17	0.09	–0.26	0.17	–1.54
Altitude (m)	<1000	0.00	2.12	0.00	0.00	0.02	0.00	0.00	0.00
	1000–1600	18.41	16.77	1.10	0.64	–0.02	0.66	0.20	3.25
	1600–2200	66.87	37.71	1.77	0.31	–0.63	0.94	0.17	5.63
	2200–2800	13.50	25.84	0.52	–0.54	0.15	–0.69	0.23	–3.02
	>2800	1.23	17.56	0.07	–2.16	0.18	–2.35	0.71	–3.30
Distance to rivers (m)	0-200	18.41	17.96	1.03	0.04	–0.01	0.05	0.20	0.23
	200–400	24.54	16.21	1.51	0.54	–0.11	0.64	0.18	3.51
	400–600	15.34	14.35	1.07	0.31	–0.01	0.32	0.22	1.47
	600–800	15.34	12.97	1.18	0.51	–0.03	0.54	0.22	2.47
	>800	26.38	38.52	0.69	–1.13	0.18	–1.31	0.18	–7.34
Distance to roads (m)	0–1000	31.29	11.52	2.72	1.15	–0.25	1.40	0.17	8.29
	1000–1800	9.20	7.77	1.18	0.71	–0.02	0.73	0.27	2.69
	1800–2600	12.88	6.46	2.00	1.42	–0.07	1.49	0.23	6.38
	2600–3400	5.52	5.62	0.98	0.85	0.00	0.85	0.34	2.47
	>3400	41.10	68.63	0.60	–2.15	0.63	–2.78	0.16	–17.45

Table 2. (continued)

Factors	Classes	Percentage of landslide (%)	Percentage of domain (%)	Frequency ratio	W^+	W^-	C	$S(C)$	$C/S(C)$
Lithology	A	12.88	34.41	0.37	–0.98	0.28	–1.27	0.23	–5.42
	B	0.61	2.83	0.22	–1.53	0.02	–1.55	1.00	–1.55
	C	9.82	15.21	0.65	–0.44	0.06	–0.50	0.26	–1.90
	D	66.26	20.23	3.28	1.19	–0.86	2.05	0.17	12.36
	E	7.36	14.35	0.51	–0.67	0.08	–0.75	0.30	–2.49
	F	3.07	8.57	0.36	–1.03	0.06	–1.09	0.45	–2.39
	G	0.00	3.32	0.00	0.00	0.03	0.00	0.00	0.00
	H	0.00	1.09	0.00	0.00	0.01	0.00	0.00	0.00
Rainfall	<300 mm/yr	3.68	22.57	0.16	–2.33	0.22	–2.55	0.42	–6.13
	300–400 mm/yr	18.41	25.62	0.72	–0.98	0.09	–1.07	0.20	–5.29
	400–500 mm/yr	24.54	5.51	4.45	2.39	–0.23	2.61	0.18	14.34
	500–600 mm/yr	53.37	25.36	2.11	0.11	–0.47	0.58	0.16	3.70
	>600 mm/yr	0.00	20.94	0.00	0.00	0.24	0.00	0.00	0.00
NDVI	<–0.084	0.00	0.00	0.00	0.00	0.00	0.00	0.00	0.00
	–0.084 – –0.020	19.02	25.40	0.75	–0.29	0.08	–0.37	0.20	–1.86
	–0.020–0.043	69.33	64.61	1.07	0.07	–0.14	0.21	0.17	1.26
	>0.043	11.66	9.99	1.17	0.15	–0.02	0.17	0.24	0.71
STI	<5	42.95	32.01	1.34	0.29	–0.18	0.47	0.16	2.97
	5–10	20.25	19.74	1.03	0.03	–0.01	0.03	0.20	0.16
	10–15	13.50	12.45	1.08	0.08	–0.01	0.09	0.23	0.41
	>15	23.31	35.80	0.65	–0.43	0.18	–0.61	0.19	–3.28

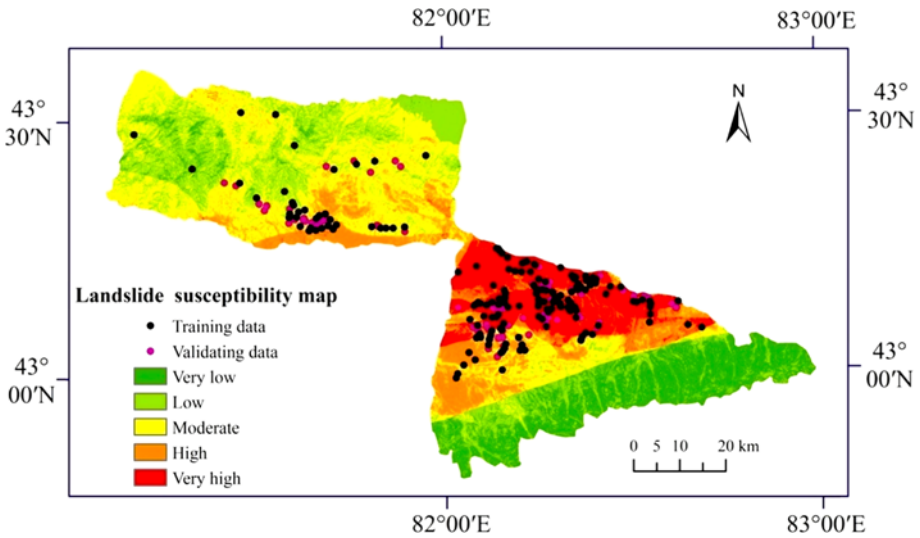

Fig. 4. Landslide susceptibility map derived from the ANN model.

and very high susceptibility zones represent 27.32, 19.15 and 12.58% of the total area, respectively. Meanwhile, the results show that the percentages of the total landslides in very low, low, moderate, high, and very high susceptibility classes are 0, 3.86, 17.17, 27.04, and 51.93%, respectively (Table 3).

5.2. Weights of Evidence (WoE) Model

Every parameter map is crossed with the landslide inventory map based on the weights of evidence model using the ArcGIS 10.0 software. The resulting total weights, as shown in Table 2, directly indicate the importance of each factor. In the case of slope angle, slope class 0–16 shows a good positive relationship with the occurrence of landslides. The slope aspects of south are more susceptible to landslides. This is likely due to the orientation of the main valley, which makes the slopes with south aspect drier while resulting in less natural vegetative cover and making the slopes unstable. The results show that

Table 3. Comparison of predicted landslide hazard zones and observed landslides

Landslide susceptible zones	ANN model		WoE model	
	Area (%)	Landslide (%)	Area (%)	Landslide (%)
Very high	12.58	51.93	8.88	42.49
High	19.15	27.04	14.29	19.31
Moderate	27.32	17.17	22.73	23.61
Low	24.37	3.86	31.44	12.45
Very low	16.58	0	22.66	2.15

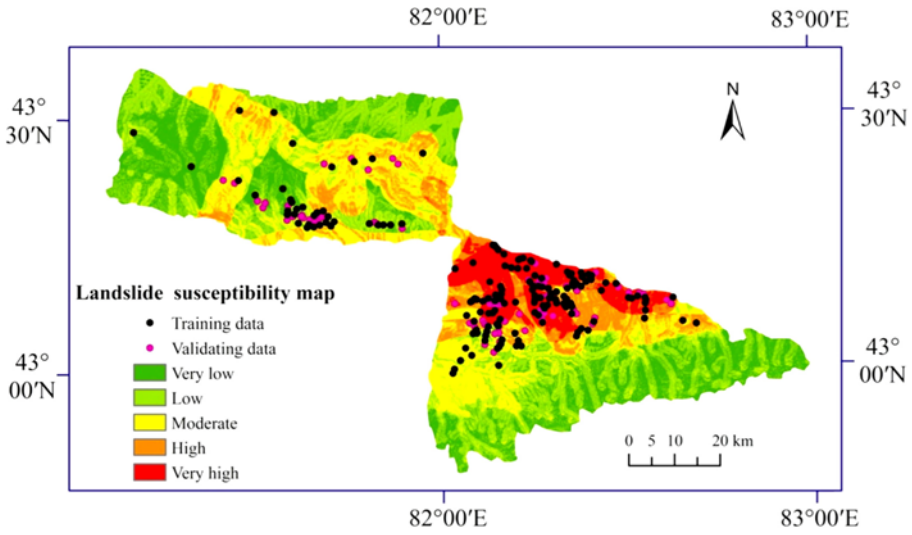

Fig. 5. Landslide susceptibility map derived from the WoE model.

general curvature, plan curvature, and profile curvature is not a very sensitive predicting factor in this area because the weights for each class were similar. But, relatively speaking, general curvature <–0.05, plan curvature >0.05, and profile curvature <–0.05 have the high influence in triggering landslides. Altitudes between 1,600 and 2,200 m were shown to have the highest studentized contrast, indicating that this category is most susceptible to landslides. In the case of distance from rivers, the weight value is higher in the class 200–400 m and lower in the class >800 m, indicating a lower probability of landslides farther to rivers. Also distance from roads also has a clear influence on landslides, because at a distance of <1,000 m the contrast is much higher than for the other classes, indicating a lower probability of landslides further away from the roads. The influence of lithology is also very evident as the contrast is highest for the lithological unit of the carbonate, clastic rocks, glutenite, limestone, rhyolitic porphyry, and basaltic porphyrite, and lowest (negative) for lithological unit of the cohesive soil, sand gravel, pebbles, loess and gravel. In the case of rainfall, the classes 400–500, 500–600 mm/year have higher values, that is, the landslide susceptibility is higher in these ranges. The relation between NDVI and landslide probabilities showed that the class of –0.020–0.043 has a high value indicating that the probability of occurrence of landslide in this normalized difference vegetation index is high. Similarly, for sediment transport index, the weight was high in <5 class, which indicates a high probability of landslide occurrence.

In this study, the final calculated LSI values of the area for WoE model range from about –50.70 to 56.55. The LSI on the produced maps was grouped into five classes (very low, low, moderate, high, and very high) using the natural break method (Fig. 5). According to this model, 8.88% of the area is exposed to a very high susceptibility, and 14.29%, 22.73%, 31.44% and 22.66% occupies high, moderate, low and very low, respectively. It can be observed from Table 3 that 2.15% and 12.45% of the total landslides falls in the very low and low susceptibility zones respectively. Moderate, high, and very high susceptible zones represent 23.61%, 19.31%, and 42.49% of the landslides, respectively.

5.3. Validation of the Landslide Susceptibility Maps

The critical strategy in prediction models is the task of validating the predicted results that can provide meaningful interpretation of the results (Pourghasemi et al., 2013c). The landslide susceptibility maps derived by two models were tested using the area under curve (AUC) method. This method works by creating specific rate curves (i.e., success- and prediction-rate curves) which explains percentage of known landslides that fall into each defined level of susceptibility rank and displays as the cumulative frequency diagram (Chung and Fabbri, 2003; Intarawichian et al., 2011). In this process,

the success rate curve is based on a comparison of the susceptibility map with the landslides used in modeling (i.e., the training set) and the prediction rate curve can be created by the validation landslide inventory (Pradhan and Kim, 2014). In rate curve, the *y* axis is normally considered as the cumulative percentage of observed landslide occurrences in different susceptibility classes and the *x* axis corresponds to the cumulative percentage of the area of the susceptibility classes. Total area under a rate curve (AUC) can be used to determine prediction accuracy of the susceptibility map qualitatively in which larger area means higher accuracy achieved (Lee, 2005b; Mathew et al., 2009; Intarawichian et al., 2011; Pourghasemi et al., 2013b). In this study, of the 233 landslides identified, 163 (70%) locations were used for the landslide susceptibility maps, while the remaining 70 (30%) cases were used for the model validation. Then success- and prediction-rate curves were constructed by using the training dataset 70% (163 landslide locations) and the remaining 30% (70 landslide locations) cases respectively, and their respective areas under the curve, AUC, were calculated to generate the comparisons.

The success rate curves of artificial neural network and weight of evidence models shown in Figure 6a. It could be observed that the artificial neural network model have the higher area under the curve (AUC) values (0.8251) than the weight of evidence model (0.7982). Similarly, the prediction rate curves (Fig. 6b) showed that in the susceptibility map using the artificial neural network model, the AUC was 0.7731. In the susceptibility map using weight of evidence model, the AUC was 0.7459. Therefore, it was found that the training accuracy of the susceptibility maps was 82.51% and 79.82% for ANN and WoE models, respectively. The overall prediction rates for the ANN and WoE models were 77.31% and 74.59% respectively. Thus, it can be concluded that the area under the curve (AUC) for both the success rate and prediction rate curves of the ANN and WoE models showed that both models are successful estimators, and the two models employed in this study have reasonably good accuracy in predicting the landslide susceptibility of the study area. In addition, the ANN model was deemed to be more efficient for landslide susceptibility mapping of the study area.

6. CONCLUSIONS

In this study, two landslide susceptibility mapping models, the artificial neural network and weight of evidence models, were applied to Xinjiang Uygur Autonomous Region, China, as the study area, using a GIS for estimating the susceptible areas of the study area. The selection of the twelve conditioning landslide factors including slope angle, slope aspect, general curvature, plan curvature, profile curvature, altitude, distance to rivers, distance to roads, lithology, rainfall, NDVI, and STI, based on consideration of relevance, availability, and scale of data that was available for the study area, is relative and subjective, and can be improved in future research. The susceptibility maps produced by ANN and WoE models were divided into five different susceptibility classes such as very low, low, moderate, high, and very high. The validation has been determined by using the area under the rate curve method in which the accuracy of the LS maps produced by the ANN and WoE models was 82.51% and 79.82%, respectively for success rate technique and was 77.31% and 74.59%, respectively for predictive rate technique. Overall, both models showed almost similar results and were reasonable models for the landslide susceptibility mapping of the study area. Meanwhile, it can be observed that the landslide occurrence potential map produced by the ANN method is highly believable, because the method's high and very high landslide occurrence potential classes correctly predicted most of the observed landslides. In addition, it should be noted that both the models were developed on some basic assumptions such as topography, geology, and stream etc. if data no factors causing the landslides, such as extreme rainfall, earthquake shaking, exist, then a more accurate analysis could be done. The results and findings of the present study can help the

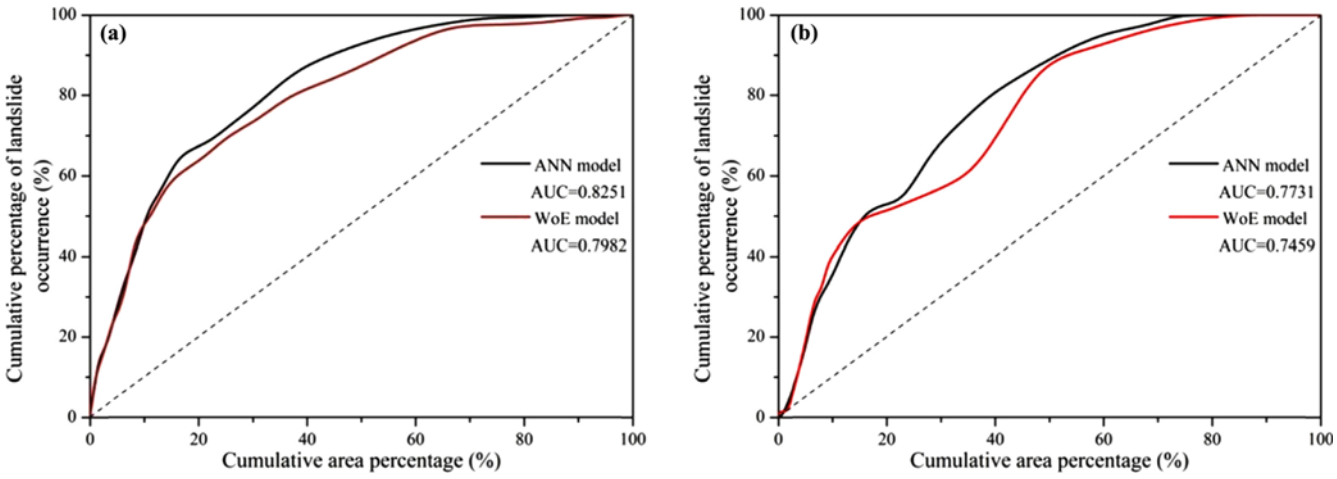

Fig. 6. AUC representing quality model (a) success rate curve and (b) prediction rate curve.

developers, planners, and engineers for slope management and land-use planning. Also, it is worth mentioning that the similar method can be used elsewhere where the same geological and topographical feature prevails.

ACKNOWLEDGMENTS: The authors would like to express their gratitude to everyone who provided assistance for the present study. The study is jointly supported by the National Program on Key Basic Research Project (Grant No. 2015CB251601) and the State Key Program of National Natural Science of China (Grant No. 41430643). The authors would also like to acknowledge anonymous reviewers and editor for their helpful comments on the previous version of the manuscript.

REFERENCES

Agterberg, F.P., Bonham-Carter, G.F., Cheng, Q., and Wright, D.F., 1993, Weights of evidence modeling and weighted logistic regression for mineral potential mapping. Computers in geology, 25, 13–32.

Ahmed, B., 2014, Landslide susceptibility mapping using multi-criteria evaluation techniques in Chittagong Metropolitan Area, Bangladesh. Landslides, 12, 1–19.

Akgun, A., 2012, A comparison of landslide susceptibility maps produced by logistic regression, multi-criteria decision, and likelihood ratio methods: a case study at İzmir, Turkey. Landslides, 9, 93–106.

Akgun, A., Dag, S., and Bulut, F., 2008, Landslide susceptibility mapping for a landslide-prone area (Findikli, NE of Turkey) by likelihood-frequency ratio and weighted linear combination models. Environmental Geology, 54, 1127–1143.

Akgun, A., Sezer, E.A., Nefeslioglu, H.A., Gokceoglu, C., and Pradhan, B., 2012, An easy-to-use MATLAB program (MamLand) for the assessment of landslide susceptibility using a Mamdani fuzzy algorithm. Computers & Geosciences, 38, 23–34.

Armaş, I., 2012, Weights of evidence method for landslide susceptibility mapping. Prahova Subcarpathians, Romania. Natural Hazards, 60, 937–950.

Ayalew, L. and Yamagishi, H., 2005, The application of GIS-based logistic regression for landslide susceptibility mapping in the Kakuda-Yahiko Mountains, Central Japan. Geomorphology, 65, 15–31.

Bagher-Ebadian, H., Jafari-Khouzani, K., Mitsias, P.D., Soltanian-Zadeh, H., Chopp, M., and Ewing, J.R., 2009, Predicting final extent of ischemic infarction using an artificial neural network analysis of multiparametric MRI in patients with stroke. Proceedings of the IEEE-INNS-ENNS International Joint Conference on neural networks (Abstract), Atlanta, June 14–19, p. 229–235.

Biswajeet, P. and Saro, L., 2007, Utilization of optical remote sensing data and GIS tools for regional landslide hazard analysis using an artificial neural network model. Earth Science Frontiers, 14, 143–151.

Bonham-Carter, G.F., Agterberg, F.P., and Wright, D.F., 1988, Integration of geological datasets for gold exploration in Nova Scotia. Photogrammetric Engineering and Remote Sensing, 54, 1585–1592.

Bui, D.T., Pradhan, B., Lofman, O., Revhaug, I., and Dick, O.B., 2012b, Landslide susceptibility assessment in the Hoa Binh province of Vietnam: a comparison of the Levenberg–Marquardt and Bayesian regularized neural networks. Geomorphology, 171, 12–29.

Bui, D.T., Pradhan, B., Lofman, O., Revhaug, I., and Dick, O.B., 2012a, Spatial prediction of landslide hazards in Hoa Binh province (Vietnam): a comparative assessment of the efficacy of evidential belief functions and fuzzy logic models. Catena, 96, 28–40.

Choi, J., Oh, H.J., Lee, H.J., Lee, C., and Lee, S., 2012, Combining landslide susceptibility maps obtained from frequency ratio, logistic regression, and artificial neural network models using ASTER images and GIS. Engineering Geology, 124, 12–23.

Chung, C.J.F. and Fabbri, A.G., 2003, Validation of spatial prediction models for landslide hazard mapping. Natural Hazards, 30, 451–472.

Constantin, M., Bednarik, M., Jurchescu, M.C., and Vlaicu, M., 2011, Landslide susceptibility assessment using the bivariate statistical analysis and the index of entropy in the Sibiciu Basin (Romania). Environmental Earth Sciences, 63, 397–406.

Dahal, R.K., Hasegawa, S., Nonomura, A., Yamanaka, M., Masuda, T., and Nishino, K., 2008, GIS-based weights-of-evidence modelling of rainfall-induced landslides in small catchments for landslide susceptibility mapping. Environmental Geology, 54, 311–324.

Dai, F.C. and Lee, C.F., 2002, Landslide characteristics and slope instability modeling using GIS, Lantau Island, Hong Kong. Geomorphology, 42, 213–228.

Dai, F.C., Lee, C.F., Li, J., and Xu, Z.W., 2001, Assessment of landslide susceptibility on the natural terrain of Lantau Island, Hong Kong. Environmental Geology, 40, 381–391.

Demir, G., Aytekin, M., Akgün, A., Ikizler, S.B., and Tatar, O., 2013, A comparison of landslide susceptibility mapping of the eastern part of the North Anatolian Fault Zone (Turkey) by likelihood-frequency ratio and analytic hierarchy process methods. Natural Hazards, 65, 1481–1506.

Devkota, K.C., Regmi, A.D., Pourghasemi, H.R., Yoshida, K., Pradhan, B., Ryu, I.C., and Althuwaynee, O.F., 2013, Landslide susceptibility mapping using certainty factor, index of entropy and logistic regression models in GIS and their comparison at Mugling–Narayanghat road section in Nepal Himalaya. Natural Hazards, 65, 135–165.

Dragićević, S., Lai, T., and Balram, S., 2015, GIS-based multicriteria evaluation with multiscale analysis to characterize urban landslide susceptibility in data-scarce environments. Habitat International, 45, 114–125.

Ercanoglu, M., Gokceoglu, C., and Van Asch, T.W., 2004, Landslide susceptibility zoning north of Yenice (NW Turkey) by multivariate statistical techniques. Natural Hazards, 32, 1–23.

Ermini, L., Catani, F., and Casagli, N., 2005, Artificial neural networks applied to landslide susceptibility assessment. Geomorphology, 66, 327–343.

Garrett, J.H., 1994, Where and why artificial neural networks are applicable in civil engineering. Journal of Computing in Civil Engineering, 8, 129–130.

Gorsevski, P.V., Jankowski, P., and Gessler, P.E., 2006, Heuristic approach for mapping landslide hazard integrating fuzzy logic with analytic hierarchy process. Control and Cybernetics, 35, 121–146.

Hecht-Nielsen, R., 1987, Kolmogorov's mapping neural network existence theorem. Proceedings of 1st IEEE international conference on neural networks (Abstract), San Diego, June, 3, p. 11–14.

He, S., Pan, P., Dai, L., Wang, H., and Liu, J., 2012, Application of kernel-based Fisher discriminant analysis to map landslide susceptibility in the Qinggan River delta, Three Gorges, China. Geomorphology, 171, 30–41.

Mush, D. and Horne, B., 1993, Progress in supervised neural net-

works: what's new since Lippman. IEEE Signal Processing Magazine, 8–39.

Intarawichian, N. and Dasananda, S., 2011, Frequency ratio model based landslide susceptibility mapping in lower Mae Chaem watershed, Northern Thailand. Environmental Earth Sciences, 64, 2271–2285.

Jaafari, A., Najafi, A., Pourghasemi, H.R., Rezaeian, J., and Sattarian, A., 2014, GIS-based frequency ratio and index of entropy models for landslide susceptibility assessment in the Caspian forest, northern Iran. International Journal of Environmental Science and Technology, 11, 909–926.

Kannan, M., Saranathan, E., and Anabalagan, R., 2013, Landslide vulnerability mapping using frequency ratio model: a geospatial approach in Bodi-Bodimettu Ghat section, Theni district, Tamil Nadu, India. Arabian Journal of Geosciences, 6, 2901–2913.

Kanungo, D.P., Sarkar, S., and Sharma, S., 2011, Combining neural network with fuzzy, certainty factor and likelihood ratio concepts for spatial prediction of landslides. Natural Hazards, 59, 1491–1512.

Kayastha, P., Dhital, M.R., and De Smedt, F., 2013a, Application of the analytical hierarchy process (AHP) for landslide susceptibility mapping: a case study from the Tinau watershed, west Nepal. Computers & Geosciences, 52, 398–408.

Kayastha, P., Dhital, M.R., and De Smedt, F., 2013b, Evaluation of the consistency of landslide susceptibility mapping: a case study from the Kankai watershed in east Nepal. Landslides, 10, 785–799.

Kayastha, P., Dhital, M.R., and De Smedt, F., 2012, Landslide susceptibility mapping using the weight of evidence method in the Tinau watershed, Nepal. Natural Hazards, 63, 479–498.

Kritikos, T. and Davies, T., 2015, Assessment of rainfall-generated shallow landslide/debris-flow susceptibility and runout using a GIS-based approach: application to western Southern Alps of New Zealand. Landslides, 12, 1051–1075.

Lee, S., 2005a, Application of logistic regression model and its validation for landslide susceptibility mapping using GIS and remote sensing data. International Journal of Remote Sensing, 26, 1477–1491.

Lee, S., 2005b, Application and cross-validation of spatial logistic multiple regression for landslide susceptibility analysis. Geosciences Journal, 9, 63–71.

Lee, S. and Choi, J., 2004, Landslide susceptibility mapping using GIS and the weight-of-evidence model. International Journal of Geographical Information Science, 18, 789–814.

Lee, S., Choi, J., and Min, K., 2002, Landslide susceptibility analysis and verification using the Bayesian probability model. Environmental Geology, 43, 120–131.

Lee, S. and Pradhan, B., 2007, Landslide hazard mapping at Selangor, Malaysia using frequency ratio and logistic regression models. Landslides, 4, 33–41.

Lee, S. and Sambath, T., 2006, Landslide susceptibility mapping in the Damrei Romel area, Cambodia using frequency ratio and logistic regression models. Environmental Geology, 50, 847–855.

Lee, S., Ryu, J.H., Min, K., and Won, J.S., 2003, Landslide susceptibility analysis using GIS and artificial neural network. Earth Surface Processes and Landforms, 28, 1361–1376.

Lee, S., Ryu, J.H., Won, J.S., and Park, H.J., 2004, Determination and application of the weights for landslide susceptibility mapping using an artificial neural network. Engineering Geology, 71, 289–302.

Liu, M., Chen, X., and Yang, S., 2014, Collapse Landslide and Mudslides Hazard Zonation. In: Sassa, K., Canuti, P., and Yin, Y. (eds.), Landslide Science for a Safer Geoenvironment. Springer International Publishing, p. 457–462.

Mathew, J., Jha, V.K., and Rawat, G.S., 2009, Landslide susceptibility zonation mapping and its validation in part of Garhwal Lesser Himalaya, India, using binary logistic regression analysis and receiver operating characteristic curve method. Landslides, 6, 17–26.

Nefeslioglu, H.A., Duman, T.Y., and Durmaz, S., 2008, Landslide susceptibility mapping for a part of tectonic Kelkit Valley (Eastern Black Sea region of Turkey). Geomorphology, 94, 401–418.

Nefeslioglu, H.A., Sezer, E., Gokceoglu, C., Bozkir, A.S., and Duman, T.Y., 2010, Assessment of landslide susceptibility by decision trees in the metropolitan area of Istanbul, Turkey. Mathematical Problems in Engineering, 2010, 901095.

Ohlmacher, G.C. and Davis, J.C., 2003, Using multiple logistic regression and GIS technology to predict landslide hazard in northeast Kansas, USA. Engineering Geology, 69, 331–343.

Ozdemir, A. and Altural, T., 2013, A comparative study of frequency ratio, weights of evidence and logistic regression methods for landslide susceptibility mapping: Sultan Mountains, SW Turkey. Journal of Asian Earth Sciences, 64, 180–197.

Paola, J.D. and Schowengerdt, R.A., 1995, A review and analysis of backpropagation neural networks for classification of remotely-sensed multi-spectral imagery. International Journal of Remote Sensing, 16, 3033–3058.

Park, S., Choi, C., Kim, B., and Kim, J., 2013, Landslide susceptibility mapping using frequency ratio, analytic hierarchy process, logistic regression, and artificial neural network methods at the Inje area, Korea. Environmental Earth Sciences, 68, 1443–1464.

Polykretis, C., Ferentinou, M., and Chalkias, C., 2015, A comparative study of landslide susceptibility mapping using landslide susceptibility index and artificial neural networks in the Krios River and Krathis River catchments (northern Peloponnesus, Greece). Bulletin of Engineering Geology and the Environment, 74, 27–45.

Pourghasemi, H.R., Jirandeh, A.G., Pradhan, B., Xu, C., and Gokceoglu, C., 2013c, Landslide susceptibility mapping using support vector machine and GIS at the Golestan Province, Iran. Journal of Earth System Science, 122, 349–369.

Pourghasemi, H.R., Moradi, H.R., and Aghda, S.F., 2013a, Landslide susceptibility mapping by binary logistic regression, analytical hierarchy process, and statistical index models and assessment of their performances. Natural Hazards, 69, 749–779.

Pourghasemi, H.R., Pradhan, B., and Gokceoglu, C., 2012, Application of fuzzy logic and analytical hierarchy process (AHP) to landslide susceptibility mapping at Haraz watershed, Iran. Natural Hazards, 63, 965–996.

Pourghasemi, H.R., Pradhan, B., Gokceoglu, C., Mohammadi, M., and Moradi, H.R., 2013b, Application of weights-of-evidence and certainty factor models and their comparison in landslide susceptibility mapping at Haraz watershed, Iran. Arabian Journal of Geosciences, 6, 2351–2365.

Poudyal, C.P., Chang, C., Oh, H.J., and Lee, S., 2010, Landslide susceptibility maps comparing frequency ratio and artificial neural networks: a case study from the Nepal Himalaya. Environmental Earth Sciences, 61, 1049–1064.

Pradhan, A.M.S., and Kim, Y.T., 2014, Relative effect method of landslide susceptibility zonation in weathered granite soil: a case study in Deokjeok-ri Creek, South Korea. Natural Hazards, 72, 1189–1217.

Pradhan, B., 2013, A comparative study on the predictive ability of the decision tree, support vector machine and neuro-fuzzy mod-

els in landslide susceptibility mapping using GIS. Computers & Geosciences, 51, 350–365.

Pradhan, B. and Lee, S., 2010a, Regional landslide susceptibility analysis using back-propagation neural network model at Cameron Highland, Malaysia. Landslides, 7, 13–30.

Pradhan, B. and Lee, S., 2010b, Delineation of landslide hazard areas on Penang Island, Malaysia, by using frequency ratio, logistic regression, and artificial neural network models. Environmental Earth Sciences, 60, 1037–1054.

Pradhan, B. and Lee, S., 2010c, Landslide susceptibility assessment and factor effect analysis: backpropagation artificial neural networks and their comparison with frequency ratio and bivariate logistic regression modelling. Environmental Modelling & Software, 25, 747–759.

Pradhan, B., 2011a, Manifestation of an advanced fuzzy logic model coupled with Geo-information techniques to landslide susceptibility mapping and their comparison with logistic regression modelling. Environmental and Ecological Statistics, 18, 471–493.

Pradhan, B., 2011b, Use of GIS-based fuzzy logic relations and its cross application to produce landslide susceptibility maps in three test areas in Malaysia. Environmental Earth Sciences, 63, 329–349.

Qin, X.M., 2007, Based on GIS landslide geological disaster hazard evaluation research-Taking Gongliu county as example. Master Thesis, Xinjiang University, Ürümqi, 45 p.

Regmi, N.R., Giardino, J.R., and Vitek, J.D., 2010, Modeling susceptibility to landslides using the weight of evidence approach: Western Colorado, USA. Geomorphology, 115, 172–187.

Rozos, D., Bathrellos, G.D., and Skillodimou, H.D., 2011, Comparison of the implementation of rock engineering system and analytic hierarchy process methods, upon landslide susceptibility mapping, using GIS: a case study from the Eastern Achaia County of Peloponnesus, Greece. Environmental Earth Sciences, 63, 49–63.

Saito, H., Nakayama, D., and Matsuyama, H., 2009, Comparison of landslide susceptibility based on a decision-tree model and actual landslide occurrence: the Akaishi Mountains, Japan. Geomorphology, 109, 108–121.

Shahabi, H., Khezri, S., Ahmad, B.B., and Hashim, M., 2014, Landslide susceptibility mapping at central Zab basin, Iran: A comparison between analytical hierarchy process, frequency ratio and logistic regression models. Catena, 115, 55–70.

Solaimani, K., Mousavi, S.Z., and Kavian, A., 2013, Landslide susceptibility mapping based on frequency ratio and logistic regression models. Arabian Journal of Geosciences, 6, 2557–2569.

Sujatha, E.R., Rajamanickam, G.V., and Kumaravel, P., 2012, Landslide susceptibility analysis using Probabilistic Certainty Factor Approach: A case study on Tevankarai stream watershed, India. Journal of Earth System Science, 121, 1337–1350.

Süzen, M.L. and Doyuran, V., 2004, Data driven bivariate landslide susceptibility assessment using geographical information systems: a method and application to Asarsuyu catchment, Turkey. Engineering Geology, 71, 303–321.

Tien Bui, D., Pradhan, B., Lofman, O., and Revhaug, I., 2012, Landslide susceptibility assessment in vietnam using support vector machines, decision tree, and Naive Bayes Models. Mathematical Problems in Engineering, 2012, 974638.

Van Westen, C.J., 2000, The modelling of landslide hazards using GIS. Surveys in Geophysics, 21, 241–255.

Van Westen, C.J., Van Asch, T.W., and Soeters, R., 2006, Landslide hazard and risk zonation—why is it still so difficult? Bulletin of Engineering Geology and the Environment, 65, 167–184.

Wang, Q., Li, W., Chen, W., and Bai, H., 2015, GIS-based assessment of landslide susceptibility using certainty factor and index of entropy models for the Qianyang County of Baoji City, China. Journal of Earth System Science, 124, 1399-1415.

Wu, C.H. and Chen, S.C., 2009, Determining landslide susceptibility in Central Taiwan from rainfall and six site factors using the analytical hierarchy process method. Geomorphology, 112, 190–204.

Xu, C., Xu, X., Dai, F., Xiao, J., Tan, X., and Yuan, R., 2012, Landslide hazard mapping using GIS and weight of evidence model in Qingshui river watershed of 2008 Wenchuan earthquake struck region. Journal of Earth Science, 23, 97–120.

Yalcin, A., Reis, S., Aydinoglu, A.C., and Yomralioglu, T., 2011, A GIS-based comparative study of frequency ratio, analytical hierarchy process, bivariate statistics and logistics regression methods for landslide susceptibility mapping in Trabzon, NE Turkey. Catena, 85, 274–287.

Yang, Z.H., Lan, H.X., Gao, X., Li, L.P., Meng, Y.S., and Wu, Y.M., 2015, Urgent landslide susceptibility assessment in the 2013 Lushan earthquake-impacted area, Sichuan Province, China. Natural Hazards, 75, 2467–2487.

Yeon, Y.K., Han, J.G., and Ryu, K.H., 2010, Landslide susceptibility mapping in Injae, Korea, using a decision tree. Engineering Geology, 116, 274–283.

Yesilnacar, E. and Topal, T., 2005, Landslide susceptibility mapping: a comparison of logistic regression and neural networks methods in a medium scale study, Hendek region (Turkey). Engineering Geology, 79, 251–266.

Yilmaz, I., 2009, Landslide susceptibility mapping using frequency ratio, logistic regression, artificial neural networks and their comparison: a case study from Kat landslides (Tokat–Turkey). Computers & Geosciences, 35, 1125–1138.

Youssef, A.M., Al-Kathery, M., and Pradhan, B., 2014a, Landslide susceptibility mapping at Al-Hasher area, Jizan (Saudi Arabia) using GIS-based frequency ratio and index of entropy models. Geosciences Journal, 19, 113–134.

Youssef, A.M., 2015, Landslide susceptibility delineation in the Ar-Rayth area, Jizan, Kingdom of Saudi Arabia, using analytical hierarchy process, frequency ratio, and logistic regression models. Environmental Earth Sciences, 73, 8499–8518.

Youssef, A.M., Pradhan, B., Jebur, M.N., and El-Harbi, H.M., 2014b, Landslide susceptibility mapping using ensemble bivariate and multivariate statistical models in Fayfa area, Saudi Arabia. Environmental Earth Sciences, 73, 3745–3761.

Zare, M., Pourghasemi, H.R., Vafakhah, M., and Pradhan, B., 2013, Landslide susceptibility mapping at Vaz Watershed (Iran) using an artificial neural network model: a comparison between multilayer perceptron (MLP) and radial basic function (RBF) algorithms. Arabian Journal of Geosciences, 6, 2873–2888.

Manuscript received July 27, 2015
Manuscript accepted January 4, 2016